

Effect of Ce doping on the structural, optical and magnetic properties of ZnO nanoparticles

Dhirendra Kumar Sharma^{1,2} · Kapil Kumar Sharma¹ · Vipin Kumar¹ · Anuradha Sharma²

Received: 19 March 2016 / Accepted: 1 June 2016 / Published online: 6 June 2016
© Springer Science+Business Media New York 2016

Abstract In the present study Zinc Oxide (ZnO) nanoparticles and Rare Earth (RE) ion Cerium (Ce) doped ZnO nanoparticles were synthesized by chemical precipitation technique. The synthesized nanoparticles were characterized by X-ray diffraction (XRD), energy-dispersive X-ray spectroscopy (EDX), transmission electron microscope (TEM), photoluminescence spectroscopy (PL), UV–visible spectroscopy and ferromagnetism behavior at room temperature. The XRD and EDX analysis revealed that Ce doped ZnO pattern matched with the ZnO pattern i.e. they exhibited hexagonal wurtzite structure and Ce ions were successfully incorporated into the ZnO nanoparticles. TEM images illustrated the average diameter of synthesized nanoparticles. The average diameter of ZnO and Ce doped ZnO nanoparticles was around 20 nm. PL measurements revealed that ZnO nanoparticles and Ce doped ZnO nanoparticles had an UV emission and a green emission while the Ce ions doping induced a red shift in the UV emission with broadening in the green emission. Direct type of transition of band gaps was confirmed by transmission spectra occurring at 3.5 and 3.2 eV respectively for ZnO nanoparticles and Ce doped ZnO nanoparticles i.e. decrease of band gap energy with doping of Ce ions in ZnO nanoparticles. The magnetization study on the Ce doped ZnO nanoparticles exposed outstanding ferromagnetism property at room temperature.

1 Introduction

During the last few decades, nanomaterials such as nanorods, nanowires and nanotubes have been the subject of extensive interest because of their potential use in a wide range of field-effect transistors [1], single-electron transistor [2], photodiodes [3, 4] and sensing application [5, 6]. The physical, chemical, magnetic, electronic and optical properties of nanomaterials can differ significantly because of large surface area to volume ratio than their bulk counterparts [7]. In addition, metal oxide nanomaterials have drawn a special attention because of inheriting the fascinating properties such as piezoelectricity, chemical sensing, photo-detection and also possess unique properties associated with their highly anisotropic geometry and size confinement [8].

Among various metal oxides, many researchers have shown much interest in ZnO and its fundamental research and practical studies because of its excellent optical, electrical, optoelectronic, gas-sensing, piezoelectric and photochemical properties [9, 10]. ZnO has a large direct band gap of ~ 3.37 eV and a high exciton binding energy of 60 meV that makes it attractive for its emission tendency in UV and full color lighting [11, 12]. Another attractive property of ZnO is photocatalysis. It is because of its non-hazardous nature and tremendous physical and chemical stability [13–17]. Its photocatalytic efficiency depends on the competition between electron–hole recombination process and surface chemical reaction. If recombination process of electron and hole occurs too fast, we find that the surface chemical reaction does not occur. Due to very fast recombination of photogenerated electron–hole pairs, the photocatalytic efficiency of ZnO remains low. Therefore, to improve the photocatalytic activity of ZnO, numerous modification techniques have

✉ Dhirendra Kumar Sharma
dhirajvasistha@gmail.com

¹ Department of Physics, Krishna Institute of Engineering and Technology, Ghaziabad, India

² Department of Physics, YMCA University of Science and Technology, Faridabad, India

been developed. In literature it has been cited that photocatalytic efficiency of semiconductor photocatalyst i.e. ZnO can be enhanced by doping certain cation which can act as electron trapping agents to decrease electron–hole recombination rate [18].

Doping is considered an effective way to enhance the properties of ZnO for various applications. There are numerous reports on the utilization of several metals for doping such as Nd [19], Sn [20], Ag [21], Mn [22], Ga [23] and Ce [13–17, 24]. In this framework, the doping of RE ion in ZnO is of great importance due to signs of tunable luminescence and ferromagnetism at room temperature.

RE ions are extensively used as activators in different host materials due to their high fluorescence efficiencies and very narrow line fluorescence bands. The ferromagnetism property of RE doped ZnO nanostructures is another such property which has drawn a great interest. These nanostructures find applications in magneto-optical device applications i.e. communications, storage, quantum computation etc. [25, 26]. Due to only few percent of doping of RE ions into non-magnetic semiconductor and to achieve ferromagnetism are known as Diluted Magnetic Semiconductor (DMS). Specifically, room temperature ferromagnetism of Ce doped ZnO nanostructures have not been reported extensively. RE doped ZnO nanomaterials i.e. nanophosphors and DMS are an attractive class of materials with ferromagnetism and optical emission from $4f-4f$ or $4f-5d$ transition of rare earth ions [24, 27]. Ce doped ZnO nanophosphors have been comprehensively studied because of the unusual interaction between the excited states and the host lattice.

CeO₂ has a band gap of 3.0 eV and possesses a unique optical characteristic for visible LED and high power laser that are similar to ZnO [11–28]. Thus, the Ce doped ZnO nanomaterials also exhibited versatile properties and have been explored to assess the photoluminescence and photoelectrochemical activity under visible light, gas-sensing properties and ferromagnetism [24, 29, 30]. So, the preparation and characterization of Ce doped ZnO nanostructures still need further research and investigation. To date, various synthesis techniques of RE doped ZnO nanostructures have been reported, including the hydrothermal method, magnetron sputter deposition, pulsed laser deposition, photolithography and wet chemical etching. In present investigation, an attempt has been made for synthesis of ZnO nanoparticles and Ce doped ZnO nanoparticles by chemical precipitation technique and studied for effect of Ce doping on properties of ZnO nanoparticles.

Though it's not an easy task to incorporate RE ions into the lattice of semiconductors that efficiently via chemical method as Ce ion has large radius and there is a noticeable

difference between their charges and chemical properties but this process was undertaken in this study effectively. In the method of synthesis of ZnO nanoparticles and Ce doped ZnO nanoparticles, the addition of reactant solutions of zinc nitrate to sodium hydroxide and zinc nitrate and cerium nitrate to sodium hydroxide begin the process of precipitation. In this technique, composition of the solvent is modified in such a way that the ZnO nanoparticles is formed, which in itself requires deep understanding of the growth mechanism of nanoparticles as ZnO has a significantly lower solubility than the concentration in solution whereas the formation of Ce doped ZnO nanoparticles made it evident that RE ion can be introduced into the ZnO nanoparticles and shift of energy from host to RE ions can be accomplished if synthesis process is well designed and charge discrepancy is compensated as per the purpose. Chemical precipitation technique is easily reproducible and applicable to large scale industrial fabrication of products at low cost.

2 Experimental procedure

In this report ZnO nanoparticles and Ce doped ZnO nanoparticles were synthesized using chemical precipitation method. All chemicals used here were of analytical grade and highly pure. In this procedure for ZnO nanoparticles 0.5 M zinc nitrate hexahydrate [Zn(NO₃)₂•6H₂O] and 0.5 M sodium hydroxide [NaOH] (as precipitant agent) were dissolved in ionized water and slowly mixed into constantly magnetic stirred. For Ce doped ZnO nanoparticles 0.5 M zinc nitrate hexahydrate [Zn(NO₃)₂•6H₂O] and 0.5 M cerium nitrate hexahydrate [Ce(NO₃)₃•6H₂O] were dissolved in ionized water. These solutions were slowly mixed in a container to produce the precipitate of Ce doped ZnO nanoparticles. In addition 0.5 M sodium hydroxide [NaOH] and methanol [CH₃OH] were also added in this solution. In both cases the precipitates were collected, washed with ionized water for several times and then separated by centrifugal method. These clean precipitates were dried at 100 °C into the electric oven for 10 h. Finally, the dried gels were sintered at 600 °C for 1 h to get ZnO nanoparticles and Ce doped ZnO nanoparticles.

XRD (Philips X'pert Materials Research X-ray diffractometer), HRTEM (Philips CM-12), PL (Perkin-Elmer LS55 Fluorescence spectrometer), UV visible (Hitachi U-3400 UV–vis spectrometer) and magnetization measurements from commercial quantum design Physical Properties Measurement System (PPMS) were used to illustrate the crystal structures, size, luminescence and magnetic properties of ZnO nanoparticles and Ce doped ZnO nanoparticles.

3 Results and discussions

3.1 XRD characterization

To examine the formation of crystal structure and crystal phase, the synthesized ZnO and Ce doped ZnO samples were examined by XRD. Figure 1 shows the XRD pattern of ZnO nanoparticles and Ce doped ZnO nanoparticles. According to the XRD result of ZnO, it can be concluded that the prominent peaks labeled at 31.74° , 34.14° , 36.25° , 47.12° , 56.12° , 62.50° , 66.24° and 67.5° correspond to the (100), (002), (101), (102), (110), (103), (200) and (112) planes respectively, confirming the formation of hexagonal zinc oxide phase. No considerable difference could be observed between the XRD patterns of ZnO and Ce doped ZnO i.e. both these XRD patterns are analogous. Hence it was analyzed that ZnO nanoparticles and Ce doped ZnO nanoparticles have hexagonal wurtzite structure and diffraction data in Fig. 1 are in agreement with the JCPDS card for ZnO (JCPDS 36-1451). Impurity peaks such as CeO_2 and CeO_3 are not observed in the XRD pattern of Ce doped ZnO nanoparticles. Due to the absence of any impurity peaks, it was clear that Ce^{+3} ions were uniformly substituted into the Zn^{+2} ions and the integration of Ce ion in the ZnO matrix has no effect in the complete crystal structure. George et al. [31] expected that the substitutional doping to change the bond distances reflected through the change in unit cell lattice parameters and the peak intensities can be affected by the change in electron density due to substitution of atoms. In addition they suggested that the

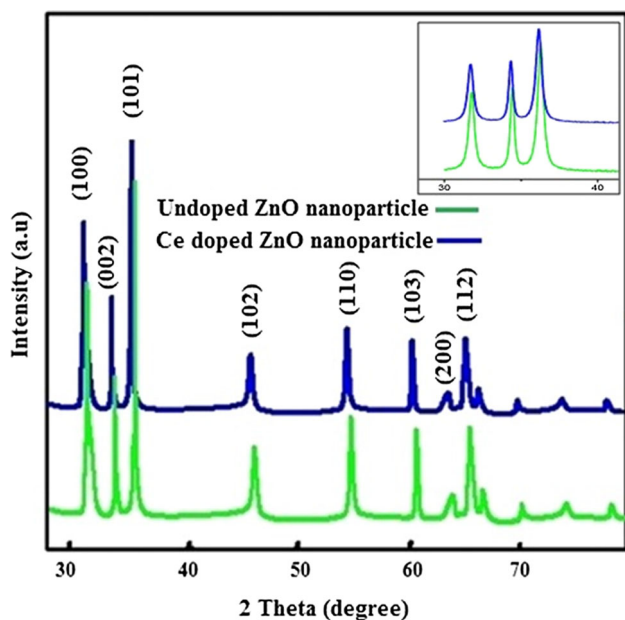


Fig. 1 X-ray diffraction pattern of ZnO nanoparticles and Ce doped ZnO nanoparticles (inset showing peak shifting toward lower angle as Ce doping)

increase in lattice parameters can be due to interstitial incorporation of Ce ions in ZnO matrix while decrease in lattice parameters can be due to replacement of Zn ions with Ce ions. In the XRD pattern (Fig. 1) of Ce doped ZnO nanoparticles prominent diffraction peaks were shift slightly towards smaller diffraction angle as compared to XRD pattern of ZnO nanoparticles. According to the reported literature this shift in the peak positions of Ce doped ZnO nanoparticles indicate in the change of lattice parameters values than ZnO nanoparticles. The lattice parameters were also calculated from these XRD patterns. The lattice parameters of Ce doped ZnO nanoparticles are $a = 3.2457$, $c = 5.2019$ and ZnO nanoparticles are $a = 3.2435$, $c = 5.1984$. The shift in the peak position of XRD data and increase in the lattice parameters reveals that Ce^{+3} ions (1.01 \AA) with bigger ionic radius have been successfully integrated into the Zn^{+2} ions (0.74 \AA) sites [11]. The formation of nanocrystalline ZnO and Ce doped ZnO were reflected through the broadening of the XRD characteristic lines for ZnO and Ce doped ZnO. So the average size of nanoparticles were calculated by using Debye–Scherrer's equation ($D = k\lambda/\beta \cos\theta$, $k = 0.99$ for spherical particles). In this equation D is the average crystallite size, λ is the X-ray wavelength, θ is the Bragg's angle and β is the full width at half maxima (FWHM) of the peak. The average size of ZnO nanoparticles and Ce doped ZnO nanoparticles was 22 nm.

3.2 EDX characterization

The contents and compositions of the Ce doped sample were studied by EDX spectra equipped in HRTEM. Figure 2 shows EDX spectra of the Ce doped ZnO nanoparticles. EDX analysis confirmed the presence of Zn, Ce and O element in the sample. The peaks of C and Cu may be

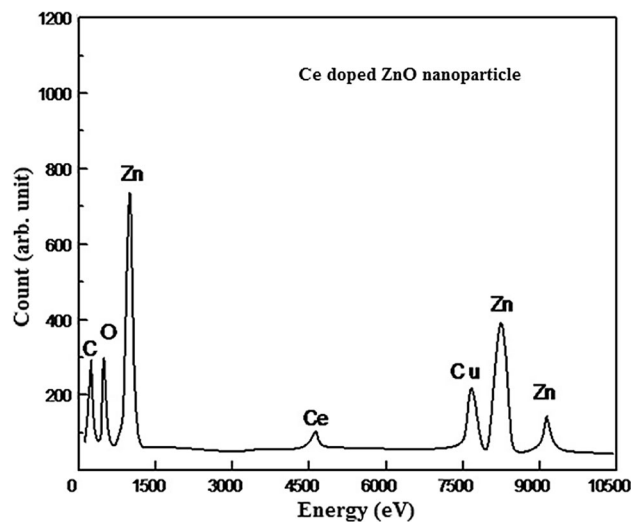


Fig. 2 EDX image of Ce doped ZnO nanoparticles

due to Cu grid. The atomic percentage of Ce in the sample was estimated as $\sim 2.0\%$ which clearly confirmed that the Ce dopant was successfully incorporated into the ZnO nanoparticles.

3.3 TEM characterization

Figure 3a, b shows the TEM images of the ZnO nanoparticles and Ce doped ZnO nanoparticles. In both the images, no considerable difference was observed. In both characterizations, almost spherical nanoparticles were observed. The average size of nanoparticles was around 20 nm. In both cases the ZnO nanoparticles and Ce doped ZnO nanoparticles were observed in the size range of 20–60 nm.

3.4 PL characterization

Figure 4 shows the PL spectra of ZnO nanoparticles and Ce doped ZnO nanoparticles. The PL spectra of ZnO nanoparticles contain two strong emission peaks at UV (388.4 nm) and visible range (535 nm). The UV emission is due to the near band–edge (NBE) emission of ZnO, which generates from the recombination of exciton–exciton

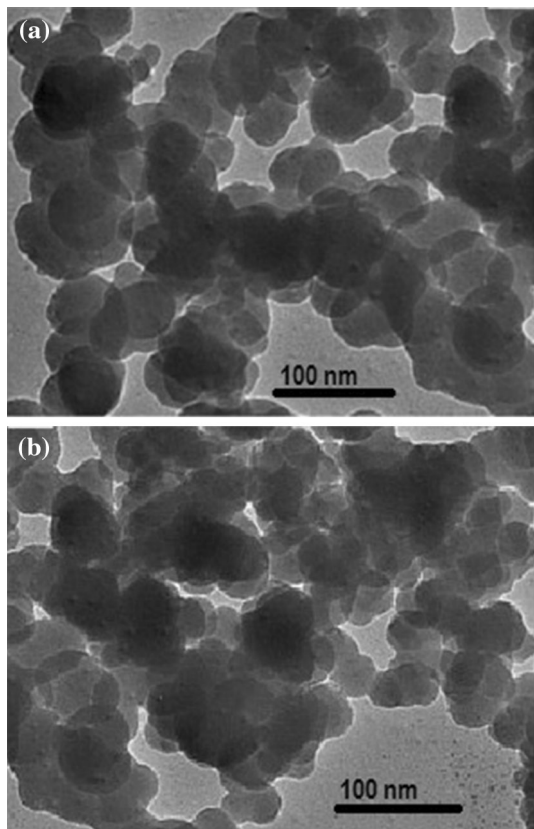


Fig. 3 **a** TEM image of ZnO nanoparticles. **b** TEM image of Ce doped ZnO nanoparticles

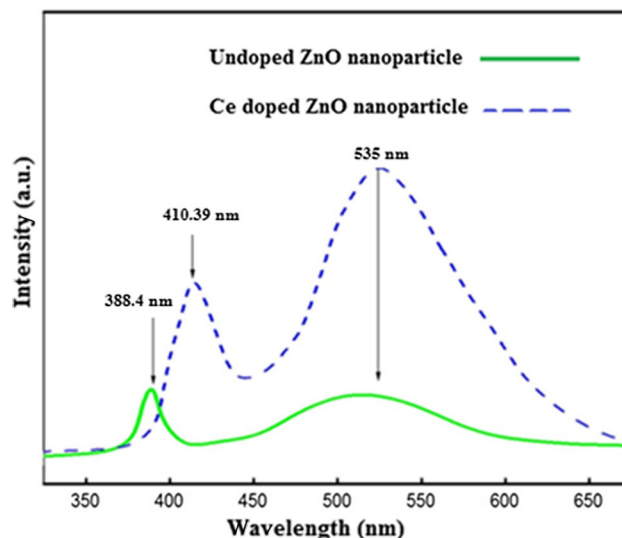


Fig. 4 PL spectra of ZnO nanoparticles and Ce doped ZnO nanoparticles

through collision process [32]. The emission in the visible range is referred to as a green emission, which is the emission outcome from the radiative recombination of a photogenerated hole with an electron occupying the oxygen vacancy. This green emission is due to the defects i.e. oxygen vacancy, zinc vacancy, oxygen interstitial, zinc interstitial. Oxygen vacancies arise in three diverse charge states: a neutral oxygen vacancy (VO), a singly ionized oxygen vacancy (VO*) and a doubly ionized oxygen vacancy (VO**) [33]. Vanheusden et al. [34] found that any singly ionized oxygen vacancies are responsible for the green luminescence in the ZnO. On comparing the PL spectrum of Ce doped ZnO nanoparticles with the peak for ZnO nanoparticles, the peak position of the UV emission shifts to a higher wavelength region (from 388.4 to 410.39 nm). The change in the peak position of UV emission is recognized to an increase in the concentration of Ce ion in ZnO nanoparticles [35]. In the PL spectra of Ce doped ZnO nanoparticles new emission spectra are developed which leads to the red shift in the UV emission [36, 37]. In addition the broad green emission also exists in the spectra which originate by Ce ion introduced into the ZnO nanoparticles i.e. electron energy transition from $5d$ to $4f$ orbital's in the Ce^{+3} ions. From this analysis Fig. 4 suggest that after doping of Ce ion in ZnO nanoparticles, the band gap of ZnO nanostructure can be tailored significantly.

3.5 UV–visible characterization

Figure 5a shows the optical transmittance spectra of the ZnO nanoparticles and Ce doped ZnO nanoparticles, which were measured at room temperature in 300–800 nm

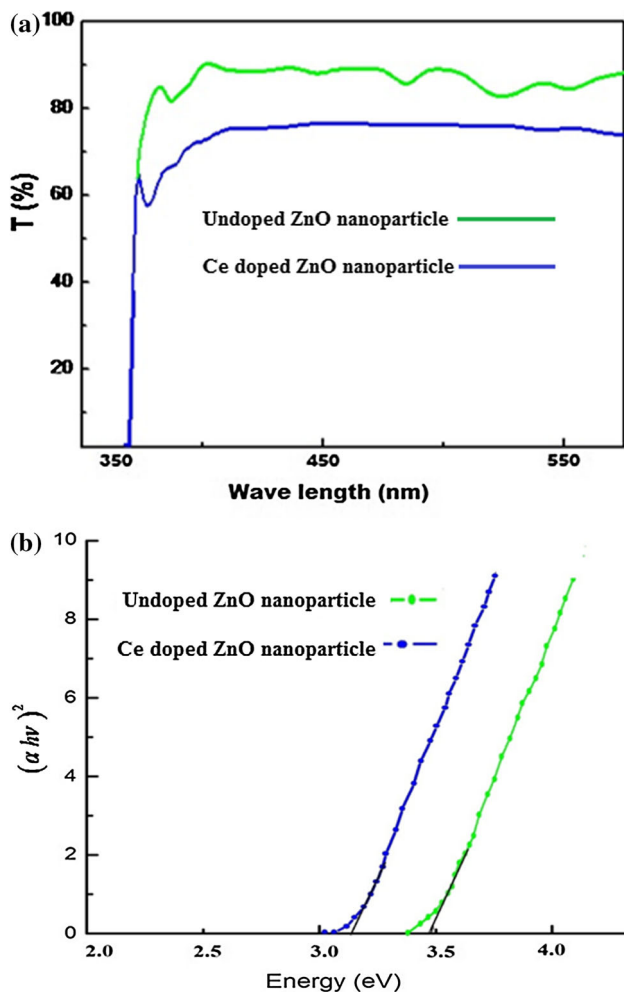


Fig. 5 **a** Transmission spectra of ZnO nanoparticles and Ce doped ZnO nanoparticles. **b** Determination of band gap of ZnO nanoparticles and Ce doped ZnO nanoparticles

wavelength range using a UV/VIS spectrophotometer. The energy band gap of the ZnO nanoparticles and Ce doped ZnO nanoparticles were calculated from the transmittance spectra using Tauc relation. For determination of band gap we have plotted a graph between $(\alpha hv)^2$ versus hv as shown in Fig. 5b. The extrapolation of straight line on the energy (hv) axis gives a band gap for ZnO nanoparticles and Ce doped ZnO nanoparticles respectively at 3.35 and 3.2 eV. This clearly indicates a significant reduction in band gap after doping of Ce ion in ZnO. The net reduction in the band gap energy, upon Ce insertion, could be due to the formation of Ce related, localized, density of states closer to the conduction band minima of ZnO. Such localized electronic states have also been reported to form the new unoccupied molecular orbitals and facilitate band gap reduction of host compound [38].

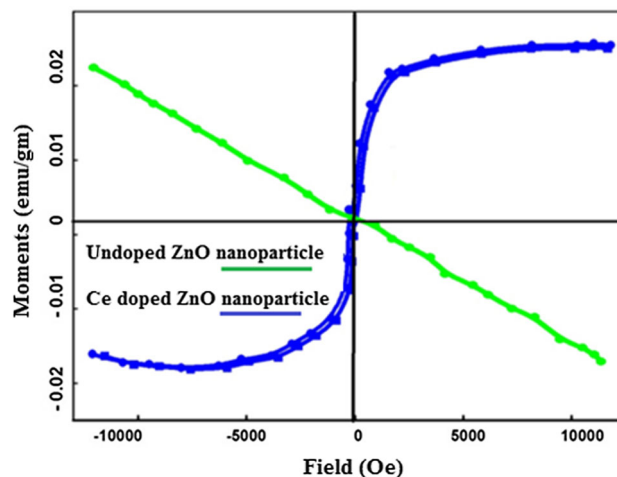


Fig. 6 Ferromagnetism curve of ZnO nanoparticles and Ce doped ZnO nanoparticles

3.6 Magnetization characterization

Figure 6 shows the magnetization curves of ZnO nanoparticles and Ce doped ZnO nanoparticles at room temperature. The ZnO nanoparticles demonstrate a diamagnetic behavior at room temperature, as indicated by magnetization curve shown in Fig. 6. It was observed that the Ce doped ZnO nanoparticles exhibit noticeable ferromagnetism at room temperature with $M_s = 0.023 \mu\text{B}/\text{Ce}$ and $H_c = 155 \text{ Oe}$, as shown in Fig. 6. The ferromagnetism at room temperature was rarely reported in the RE ions doped ZnO nanostructures [24]. To the best of our knowledge, this study is one of the preliminary description about ferromagnetism at room temperature of Ce doped ZnO nanoparticles. The faithful cause of this ferromagnetism is not until now clear due to be short of theoretical work.

RE atoms have incompletely filled $4f$ orbitals that bring magnetic moments and may get part in magnetic coupling as in the case of transition metals with incompletely filled $3d$ orbitals which are delocalized, robustly direct exchange interactions and have high Curie temperature, but regularly the orbital momentum is zero, leading to small total magnetic moment per atom [39, 40]. The $4f$ electrons are localized, exchange interactions are not direct via $5d$ or $6s$ conduction electrons, and the high orbital momentum leads to high total magnetic moments per atom. It is likely that the magnetic coupling strength of the f orbitals is much weaker than that of the d orbitals due to the stronger localization of the f electrons. Ce atom that has atomic configuration $1s^2 2s^2 2p^6 3s^2 3p^6 3d^{10} 4s^2 4p^6 4d^{10} 5s^2 5p^6 4f^5 5d^1 6s^2$ is a fascinating RE element that has equally incompletely filled $4f$ and $5d$ orbitals, which can take part in a new coupling mechanism happening via intra-ion $4f$ –

5d swap over interaction, followed by inter-ion 5d–5d coupling mediated through charge carriers to show the observed ferromagnetism [24].

4 Conclusions

To summarize, ZnO nanoparticles and Ce doped ZnO nanoparticles were synthesized by the chemical precipitation method. The XRD results exhibit that the ZnO nanoparticles and Ce doped ZnO nanoparticles were in hexagonal wurtzite phase and unnecessary Ce related compounds were not formed during the growth of Ce doped ZnO nanoparticles. EDX analysis showed the presence of the Ce ion into the ZnO lattice sites. The particle sizes estimated by TEM were in range of 20–60 nm. PL measurement of Ce doped ZnO nanoparticles revealed the red shift in the UV emission and green emission band for visible emission. UV–visible spectroscopy exhibited a considerable drop in the band gap after doping of Ce ions in ZnO nanoparticles. When observed keenly, it was found that the characteristic of ferromagnetism was prominent in Ce doped ZnO nanoparticles which was not at all visible in ZnO nanoparticles. It is projected that synthesized Ce doped ZnO nanoparticles could present a new potential application in the field of optical materials and spintronics in the future.

Acknowledgments The authors thank to Dr. J. Girish (Director, KIET, Ghaziabad) and Prof. C. M. Batra (Head, Department of Applied Sciences, KIET, Ghaziabad) for their constant support and encouragement to carry out this work.

References

- S.W. Chung, J.Y. Yu, J.R. Heath, *Appl. Phys. Lett.* **76**, 2068–2070 (2000)
- A. Notargiacomo, L. Di Gaspare, G. Scappucci, G. Mariottini, E. Giovine, R. Leoni, F. Evangelisti, *Mater. Sci. Eng., C* **23**, 671–673 (2003)
- O. Hayden, R. Agarwal, C.M. Lieber, *Nat. Mater.* **5**, 352–356 (2006)
- P. Feng, J.Y. Zhang, Q.H. Li, T.H. Wang, *Appl. Phys. Lett.* **88**, 153107–153109 (2006)
- C. Li, D. Zhang, X. Liu, S. Han, T. Tang, J. Han, C. Zhou, *Appl. Phys. Lett.* **82**, 1613–1615 (2003)
- A. Kolmakov, Y. Zhang, G. Cheng, M. Moskovits, *Adv. Mater.* **15**, 997–1000 (2003)
- E. Elssfah, C. Tang, *J. Phys. Chem. C* **111**, 8176–8179 (2007)
- J.G. Lu, P. Chang, Z. Fan, *Mater. Sci. Eng., R* **52**, 49–91 (2006)
- K.X. Yao, H.C. Zeng, *J. Phys. Chem. B* **110**, 14736–14743 (2006)
- Z.L. Wang, J. Song, *Science* **312**, 242–246 (2006)
- G.R. Li, X.H. Lu, W.X. Zhao, C.Y. Su, Y.X. Tong, *Cryst. Growth Des.* **8**, 1276–1281 (2008)
- J. Lang, Q. Han, J. Yang, C. Li, X. Li, L. Yang, Y. Zhang, M. Gao, D. Wang, *J. Appl. Phys.* **107**, 074302–074304 (2010)
- A.A. Ismail, A. El-Midany, E.A. Abdel-Aal, H. El-Shall, *Mater. Lett.* **59**, 1924–1928 (2005)
- N.F. Djaja, R. Saleh, *Mater. Sci. Appl.* **4**, 145–152 (2013)
- M. Faisal, A.A. Ismail, A.A. Ibrahim, H. Bouzid, S.A. Al-Sayari, *Chem. Eng. J.* **229**, 225–233 (2013)
- C. Karunakaran, P. Gomathisankar, G. Manikandan, *Mater. Chem. Phys.* **123**, 585–594 (2010)
- K. Singh, A.A. Ibrahim, A. Umar, A. Kumar, G.R. Chaudhary, S. Singh, S.K. Mehta, *Sens. Actuators, B* **202**, 1044–1050 (2014)
- W. Zhang, Z. Zhong, Y. Wang, R. Xu, *J. Phys. Chem. C* **112**, 17635–17642 (2008)
- G. Vijayaprasath, R. Murugan, S. Palanisamy, N.M. Prabhu, T. Mahalingam, Y. Hayakawa, G. Ravi, *J. Mater. Sci.: Mater. Electron.* **26**, 7564–7576 (2015)
- X. Jia, H. Fan, M. Afzaal, X. Wu, P. O'Brien, *J. Hazard. Mater.* **193**, 194–199 (2011)
- S. Kumar, V. Singh, A. Tanwar, *J. Mater. Sci.: Mater. Electron.* **27**, 2166–2173 (2016)
- C. Jing, Y. Jiang, W. Bai, J. Chu, A. Liu, *J. Magn. Magn. Mater.* **322**, 2395–2400 (2010)
- N. Wang, P. Li, J. Xu, C. Cui, H. Li, P. Yao, *J. Mater. Sci.: Mater. Electron.* **26**, 671–676 (2015)
- J. Iqbal, X. Liu, H. Zhu, C. Pan, Y. Zhang, D. Yu, R. Yu, *J. Appl. Phys.* **106**, 083515–083520 (2009)
- S.J. Pearton, C.R. Abernathy, M.E. Overberg, G.T. Thaler, D.P. Norton, N. Theodoropoulou, A.F. Hebard, Y.D. Park, F. Ren, J. Kim, L.A. Boatner, *J. Appl. Phys.* **93**, 1–13 (2003)
- K. Ando, *Solid State Sci.* **128**, 211–244 (2000)
- S. Shukla, E. Agorku, H. Mittal, A. Mishra, *Chem. Pap.* **68**, 217–222 (2014)
- B.C. Cheng, Y.H. Xiao, G.S. Wu, L.D. Zhang, *Adv. Funct. Mater.* **14**, 913–919 (2004)
- M. El Jouad, M.A. Lamrani, Z. Sofiani, M. Addou, T. El Habani, N. Fellahi, K. Bahedi, L. Dghoughi, A. Monteil, B. Sahraoui, S. Dabos, N. Gaumer, *Opt. Mater.* **31**, 1357–1361 (2009)
- M. Yousefi, M. Amiri, R. Azimirad, A.Z. Moshfegh, *J. Electroanal. Chem.* **661**, 106–112 (2011)
- A. George, S.K. Sharma, S. Chawla, M.M. Malik, M.S. Qureshi, *J. Alloys Compd.* **509**, 5942–5946 (2011)
- Y.W. Chen, Y.C. Liu, S.X. Lu, C.S. Xu, C.L. Shao, C. Wang, J.Y. Zhang, Y.M. Lu, D.Z. Shen, X.W. Fan, *J. Chem. Phys.* **123**, 134701–134705 (2005)
- W. Li, D. Mao, F. Zhang, X. Wang, X. Liu, S. Zou, Y. Zhu, Q. Li, J. Xu, *Nucl. Instrum. Methods Phys. Res. B* **169**, 59–63 (2000)
- K. Vanheusden, W.L. Warren, C.H. Seager, D.R. Tallant, J.A. Voigt, B.E. Gnade, *J. Appl. Phys.* **79**, 7983–7990 (1996)
- Z. Sofiani, B. Derkowska, P. Dalasiński, M. Wojdyła, S. Dabos-Seignon, M. Alaoui Lamrani, L. Dghoughi, W. Bała, M. Addou, B. Sahraoui, *Opt. Commun.* **267**, 433–439 (2006)
- A. Majid, A. Ali, *J. Phys. D Appl. Phys.* **42**, 045412 (2009)
- W. Li, Y. Wang, H. Lin, S.I. Shah, C.P. Huang, D.J. Doren, S.A. Rykov, J.G. Chen, M.A. Barteau, *Appl. Phys. Lett.* **83**, 4143–4145 (2003)
- V. Kumar, K.K. Sharma, D.K. Sharma, D.K. Dwivedi, *Optik* **126**, 3203–3205 (2015)
- H.S. Li, Y.P. Li, J.M.D. Coey, *J. Phys.: Condens. Matter* **3**, 7277–7290 (1991)
- T. Story, M. Gorska, A. Lusakowski, M. Arciszewska, W. Dobrowolski, E. Grodzicka, Z. Golacki, R.R. Galazka, *Phys. Rev. Lett.* **77**, 3447–3450 (1996)